Salient features of otoacoustic emissions are common across tetrapod groups and suggest shared properties of generation mechanisms

Christopher Bergevin[a,1], Geoffrey A. Manley[b], and Christine Köppl[b]

[a]Department of Physics & Astronomy and Centre for Vision Research, York University, Toronto, ON, M3J 1P3, Canada; and [b]Cluster of Excellence "Hearing4all," Research Center Neurosensory Science, and Department of Neuroscience, School of Medicine and Health Sciences, Carl von Ossietzky University, 26129 Oldenburg, Germany

Edited* by A. J. Hudspeth, The Rockefeller University, New York, NY, and approved February 3, 2015 (received for review September 25, 2014)

Otoacoustic emissions (OAEs) are faint sounds generated by healthy inner ears that provide a window into the study of auditory mechanics. All vertebrate classes exhibit OAEs to varying degrees, yet the biophysical origins are still not well understood. Here, we analyzed both spontaneous (SOAE) and stimulus-frequency (SFOAE) otoacoustic emissions from a bird (barn owl, *Tyto alba*) and a lizard (green anole, *Anolis carolinensis*). These species possess highly disparate macromorphologies of the inner ear relative to each other and to mammals, thereby allowing for novel insights into the biomechanical mechanisms underlying OAE generation. All ears exhibited robust OAE activity, and our chief observation was that SFOAE phase accumulation between adjacent SOAE peak frequencies clustered about an integral number of cycles. Being highly similar to published results from human ears, we argue that these data indicate a common underlying generator mechanism of OAEs across all vertebrates, despite the absence of morphological features thought essential to mammalian cochlear mechanics. We suggest that otoacoustic emissions originate from phase coherence in a system of coupled oscillators, which is consistent with the notion of "coherent reflection" but does not explicitly require a mammalian-type traveling wave. Furthermore, comparison between SFOAE delays and auditory nerve fiber responses for the barn owl strengthens the notion that most OAE delay can be attributed to tuning.

cochlear mechanics | hair cells | otoacoustic emissions | coupled oscillators | phase coherence

Numerous fundamental biophysical questions regarding cochlear mechanics remain unanswered, such as the relative dominance between viscous and inertial fluid forces affecting the stimulation of hair cells and the longitudinal coupling between them (1, 2). These aspects, combined with relative experimental inaccessibility, have led to much uncertainty with regard to the micromechanics at work in the organ of Corti, and thereby precisely how auditory information is initially peripherally encoded (i.e., forward transduction). One area in which there is broad agreement, however, is the notion of an "active" ear: A nonlinear amplification mechanism(s) (i.e., reverse transduction) boosts detection of low-level sounds and compresses a wide range of sound intensities into a narrower range of vibration magnitude (3). One manifestation of this process is the existence of otoacoustic emissions (OAEs), sounds measurable noninvasively in the external ear canal using a sensitive microphone (4). Because only healthy ears tend to emit, OAEs have had a significant clinical impact (e.g., pediatric audiology). Emissions can arise spontaneously (SOAEs) or be evoked by an external stimulus. In fact, SOAEs are commonly pointed to as salient evidence for active amplification, especially given their connections to perception such as "rippling" in audiograms (threshold microstructure), indicative of localized changes in detection thresholds (5, 6). SOAEs are, however, idiosyncratic in nature: Not all mammalian species have them, whereas several nonmammalian classes such as lizards exhibit robust activity. Humans have a high incidence of SOAEs, although some (healthy) ears have them but others do not. So, although SOAEs are not required per se for sensitive hearing, they provide a powerful and noninvasive means to study the function of the inner ear.

A common thread through vertebrate OAEs studies is that of an active oscillator, typically a stereovillar hair cell, acting as the essential transducer (3, 7–10). A comprehensive theory for SOAE generation across vertebrates is lacking, however, because knowledge of hair cell physiology has not yet been well connected to the collective behavior of the system as a whole. Vertebrate ears contain anywhere from 50 to 20,000 hair cells, all coupled together to varying degrees. Two different, and seemingly diametric, theoretical approaches explaining SOAEs have emerged. One model class considers the ear as a system of coupled nonlinear oscillators exhibiting a limit cycle (3, 11–13). Typically, these models are "local" in that a given oscillator is only directly coupled to its nearest neighbors. The other class focuses predominantly on the mammalian cochlea (14–19), where "global" coupling between elements arises from the hydromechanics that give rise to wave mechanics. One salient example is the standing wave model (16), where the peak of the traveling wave and stapes act as the two reflecting boundaries with a nonuniform gain medium in between, somewhat akin to a laser. That study predicted and verified interrelationships between spontaneous and evoked OAEs. Furthermore, acknowledging that nonmammalian ears exhibit different mechanics, Shera (16) proposed that the appearance of "standing waves" need not necessarily depend upon traveling waves along the basilar

Significance

Healthy ears not only detect sound but can emit it as well. These sounds can occur either spontaneously and continuously or in response to acoustic stimulation. Evoked emissions are increasingly used as clinical diagnostic tools. The mechanisms underlying their generation, however, are incompletely understood. In particular, otoacoustic emissions occur in a wide variety of species, from frogs to humans, suggesting basic, shared principles. Here, we analyzed both spontaneous and evoked otoacoustic emissions from a bird and a lizard. We relate these data to those from humans and suggest that otoacoustic emissions originate from similar biomechanical principles despite gross differences in the underlying anatomy of the ear.

Author contributions: C.B., G.A.M., and C.K. designed research; C.B., G.A.M., and C.K. performed research; C.B. contributed new reagents/analytic tools; C.B., G.A.M., and C.K. analyzed data; and C.B., G.A.M., and C.K. wrote the paper.

The authors declare no conflict of interest.

*This Direct Submission article had a prearranged editor.

Freely available online through the PNAS open access option.

[1]To whom correspondence should be addressed. Email: cberge@yorku.ca.

This article contains supporting information online at www.pnas.org/lookup/suppl/doi:10.1073/pnas.1418569112/-/DCSupplemental.

membrane (BM) but could arise via other mechanisms that create appropriate phase differences (e.g., delays due to tuning). Motivated by the uncertain role of BM traveling waves in nonmammals, our present goal was to exploit the large morphological differences that exist across vertebrate ears (20) to gain quantitative insight into SOAE generation mechanisms.

Here we focus on two different nonmammalian species: a bird, the barn owl, and a lizard, the green anole. Both species exhibit robust OAE activity (21–25). The barn owl (*Tyto alba*), is known for its remarkable ability to hunt by auditory cues alone (26). The peripheral auditory morphology, neurophysiology, and psychophysics of this species have been well characterized (27–30). Owl auditory nerve fiber (ANF) responses show average frequency tuning but have remarkably high phase-locking capabilities extending out to 10 kHz (31). Furthermore, the tonotopic map along the basilar papilla (in contrast to the mammalian organ of Corti) is nonexponential, with representation of higher frequencies (5–10 kHz) greatly expanded. The role of BM waves is unknown in owls, although data from pigeons are suggestive of their existence in birds (32). The inner ear of lizards is profoundly different from that of both humans and barn owls. In anoles, the short auditory papilla (~0.5 mm) contains ~150 hair cells and has no overlying tectorial membrane over the SOAE-producing cells (33). Bundle orientations for hair cells in a given radial cross-section are arranged in a self-opposing fashion. Furthermore, there is ample evidence indicating a lack of a traveling wave on the BM (34, 35). In this study, we systematically explored interrelationships within individual ears between SOAEs and stimulus frequency emissions (SFOAEs), the simplest type of evoked emission via a single low-level stimulus tone (15). In short, we found that important OAE characteristics are shared between the two species and with published data from humans. This we interpret as revealing generic features of the underlying active processes.

Results

Recording of OAEs is relatively straightforward, because the acoustic measurements chiefly require only light anesthesia (to prevent movement) and a sensitive microphone (*Methods*). To illustrate the general nature of the results, Fig. 1 focuses on data from a single barn owl ear. Similar data from another owl and lizard (i.e., *Anolis*) are included in Figs. S1 and S2, illustrating the degree of intersubject variability. All animals tested showed SOAE activity, usually apparent as a rippling pattern atop the microphone noise floor. In the majority of ears, at least one or more large distinct peaks were also observed. For example, the owl ear shown in Fig. 1*A* (black trace) was determined to have 12 SOAE peaks. Typically we observed SOAE activity up to ~11–12 kHz in the owl and ~5–6 kHz in the anole. Altogether, 115 peaks were identified across 15 unique owl ears, with center frequencies ranging from 3.1 to 10.6 kHz. The mean interpeak spacing for owls using this approach was 0.45 ± 0.24 kHz (mean ± SD). Dynamic properties of SOAE peaks typically indicated the presence of self-sustained sinusoids and not filtered noise (Figs. S3 and S4; human data are also included in Fig. S5 for comparison) (16, 24, 36). SOAE peaks from the owl were relatively noisy, however, possibly partly related to muscular activity such as heart beat (37).

The pressure measured in response to an external (probe) tone had two salient features when swept across frequency at a constant level. First, there was a strong oscillatory pattern to the microphone pressure at the probe frequency (red curves in Fig. 1*A*), indicative of interference between the tone and the relatively delayed emission evoked from the ear (15, 23, 38, 39). Frequency regions demonstrating greater interference typically exhibited robust SOAE activity (Fig. 1*A* and Figs. S1*A* and S2). Second, tones created a localized suppressive effect of SOAE activity (Fig. 1*B*) (6).

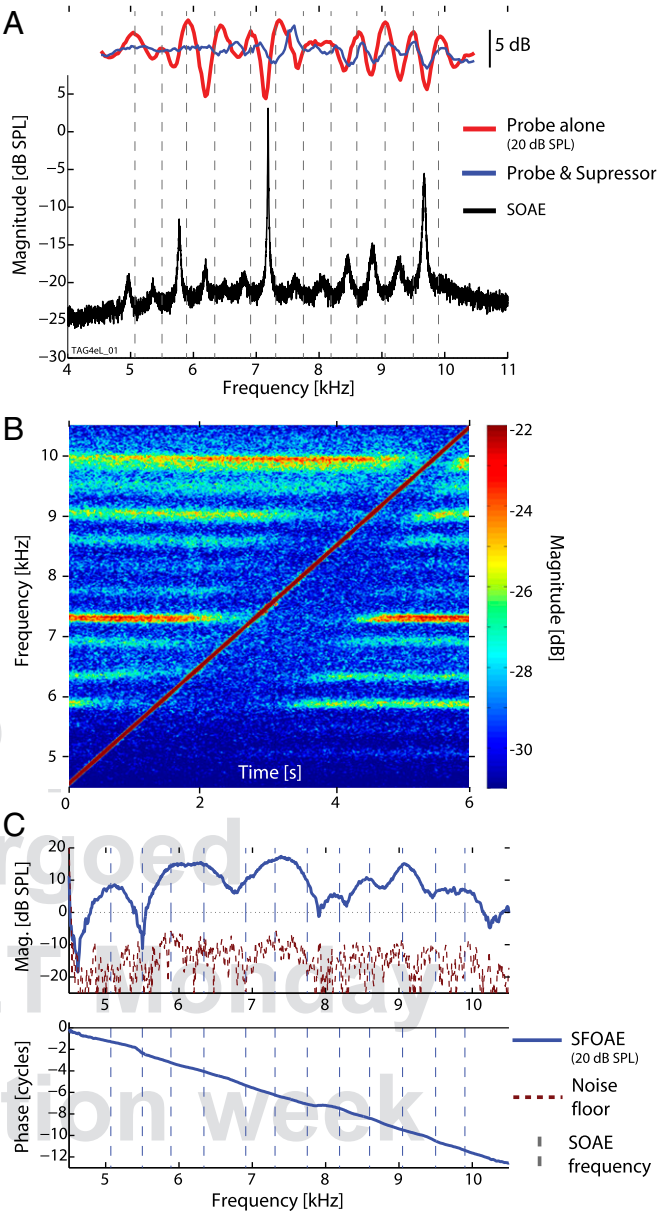

Fig. 1. Data from a representative barn owl ear. (*A*) SOAE spectrum (black curve), in the absence of any stimuli just before the SFOAE run. From the SFOAE run, the red and blue traces show the microphone response at the probe frequency when the tone was presented at a constant level ($L_p = 20$ dB SPL) for two conditions: probe alone (red curve) and probe and suppressor (blue; suppressor level 35 dB SPL and 40 Hz higher in frequency). An interference pattern is apparent owing to interaction with SOAE activity. Vertical dashed gray lines indicate the SOAE frequencies as measured during the SFOAE run [started several minutes after the initial SOAE recording shown; note upward frequency shift, presumably due to minor changes in body temperature (25)]. (*B*) Spectrogram showing effect of the tone (apparent as the diagonal trace) as it was swept across frequency during the SFOAE run. This was obtained from the probe-alone segment of the SFOAE measurement. SOAE peaks appear as horizontal bands. (*C*) Extracted SFOAE magnitude and (unwrapped) phase ($L_p = 20$ dB SPL), along with SOAE frequencies (dashed lines, as in *A*).

To measure SFOAEs, swept tones were presented in two different conditions (15, 40, 41): a single probe tone alone, or with the addition of a second "suppressor" tone slightly higher in level and nearby in frequency. Consider that in the probe-alone condition (red trace in Fig. 1*A*) the measured pressure at the stimulus

frequency is a combination of both the stimulus and the emission. When the suppressor is also presented (blue trace), the interference at the probe frequency diminishes, indicating greater dominance of the stimulus. SFOAEs were extracted by comparing the complex-valued spectral response at the probe frequency between the two conditions (15). The residual (i.e., the SFOAE) is shown in Fig. 1*C*. The magnitude indicates the size of the emission and the slope of the phase curve with respect to frequency reveals the delay (also called the phase-gradient delay). For owls, the probe level used was 20 dB SPL (sound pressure level), whereas for anoles it was 30 dB SPL to improve the signal-to-noise ratio (SNR).

All ears exhibited robust SFOAEs (i.e., SNR ≥20 dB over a broad frequency range), regardless of whether robust SOAE activity was detected. SFOAE magnitudes showed an irregular, but stable/repeatable, frequency pattern unique to a given ear. Mostly, but not always, SOAE peak frequencies corresponded to SFOAE maxima (e.g., Fig. 1*C* and Fig. S1*C*). We note that rippling was sometimes apparent in the microphone response during the probe and suppressor condition (blue trace in Fig. 1*A*), suggesting that the emission component was not always completely suppressed by our protocol. For the owl, SFOAE phase-gradient delays were relatively constant at ∼2 ms across frequency from 1 to 8 kHz (e.g., Figs. 1*C* and 2*A* and Fig. S6*A*) but decreased slightly at higher frequencies. Delays for the anole decreased from ∼4 ms to 2 ms from 0.5 to 2.5 kHz but were relatively constant above that frequency (Fig. 2*C*). For both species, we observed that localized variations in the delay were apparent. In many cases, but not always, the delay increased about SOAE peaks (e.g., Fig. 2*C* and Fig. S6), especially near larger-amplitude SOAEs. This observation is similar to that reported for humans (42). SFOAE delays can also be plotted as the dimensionless number of stimulus periods (N_{SFOAE}), as in Fig. 2 *A* and *C*.

Previous studies of mammals (43, 44) and lizards (45) have indicated that SFOAE delays are directly connected to auditory frequency selectivity, as measured by single ANF tuning curves. The barn owl presents an opportunity to test this for a bird species, because ANF tuning (Q_{ERB}, where larger Q_{ERB} means sharper tuning; *Methods*) has been well characterized (29). This interrelationship between SFOAE and neural tuning is shown in Fig. 2 *A* and *B*. Both measures (N_{SFOAE} and Q_{ERB}) increase with frequency, but at differing rates. Shown in Fig. 2*B*, the owl's "tuning ratios" (Q_{ERB}/N_{SFOAE}) may differ from those for mammals (43) because they exhibit a nonmonotonic bend around 6–7 kHz (although uncertainties increase at those higher frequencies). Although not explored here in detail, we note that varying the probe level (0–50 dB SPL) revealed frequency-dependent nonlinear aspects of SFOAE growth, with nonmonotonic regions of SFOAE magnitude typically corresponding to areas about pronounced SOAE activity (e.g., Fig. S7). SFOAE phase-gradient delays were roughly constant with respect to L_p at lower levels (≤30 dB SPL) but exhibited a marked decrease above moderate levels (≥40 dB SPL; Fig. S7), similar to humans (46, 47). For this reason, the tuning ratios are shown for two different probe levels in Fig. 2*B*. The $L_p = 20$ dB SPL case is closer to the levels used around the tips of ANF threshold tuning curves (29).

We now focus on another measure, the accumulation of SFOAE phase between adjacent SOAE peaks. The relationship between SFOAE phase and SOAE peak frequencies can be quantified in two different ways. First, shown in Fig. 2*A* (owl) and Fig. 2*C* (lizard) is a comparison between N_{SFOAE} and a measure of SOAE interpeak spacing N_{SOAE}, defined as the geometric mean frequency of an SOAE peak pair divided by their frequency separation (16). In general, N_{SOAE} and N_{SFOAE} were comparable, although N_{SOAE} were typically larger. Second, as visually motivated in Fig. 1*C*, the phase difference can be explicitly calculated, as shown in Fig. 3. Accumulation (modulo one cycle) tended to cluster about integral numbers (typically one) for owls and slightly less than for anoles (compare resultant vectors in

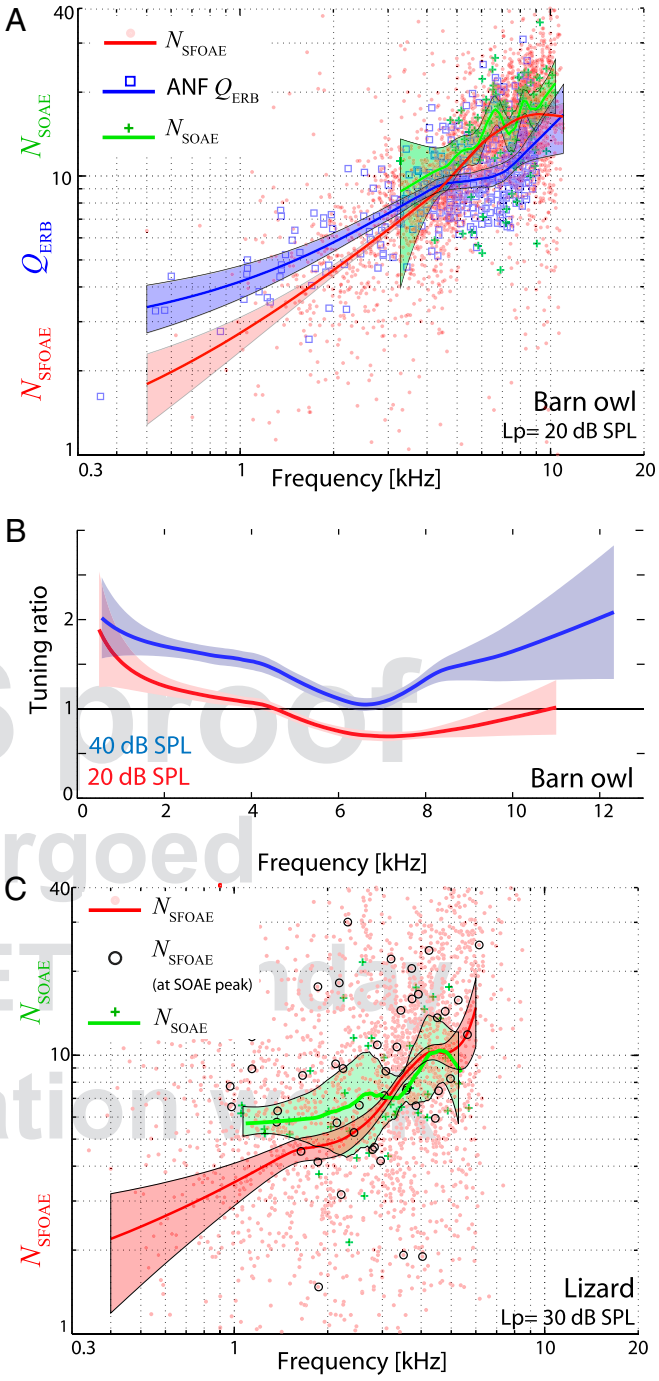

Fig. 2. (*A*) Comparison of neural tuning, SFOAE delay, and SOAE spacing for the barn owl. ANF threshold tuning (Q_{ERB}) is shown in blue, SFOAE delays (N_{SFOAE}) in red ($L_p = 20$ dB SPL), and SOAE interpeak spacing (N_{SOAE}) in green. Owl data are pooled across all nine owls and 15 ears examined, for a total of 115 SOAE peaks. (*B*) The tuning ratio [$\equiv Q_{ERB}/N_{SFOAE}$ (40)] for the barn owl is shown for two different L_p values: 20 (red) and 40 dB SPL (blue). For all plots, solid lines indicate locally weighted regression trends, and shaded regions indicate 95% confidence interval estimates obtained via bootstrapping. Note that extrapolation was used for the ANF trend above 9 kHz. (*C*) Similar comparison of N_{SFOAE} and N_{SOAE} for anoles (Q_{ERB} is unknown for this species). For the SFOAEs ($L_p = 30$ dB SPL), all N_{SFOAE} values are shown in red, and those only at determined SOAE peaks are shown as black circles. Anole data are from six unique ears from as many individuals, with a total of 52 peaks observed.

Fig. 3), relatively independent of frequency (Fig. S8). This accumulation effect was robust—unwrapping had negligible effect (Fig. 3) and adding a small dither (i.e., 10–20 Hz) to the specified SOAE frequencies did not strongly affect clustering. The distributions were significantly different from a uniform one for both owls (Kolmogorov–Smirnov test; $P < 0.001$, $D = 0.24$) and anoles ($P < 0.001$, $D = 0.3$). These measures are similar to those previously observed for humans (47). Using a one-sample t test with specified mean direction 0 (i.e., an integral number of cycles of phase accumulation) (48), the hypothesis that the mean was different could be rejected for the owl, whereas it could not be for the anole. Using a two-sample Watson–Williams test (48), the two species' (unwrapped) distributions differ in their mean angle ($P < 0.007$).

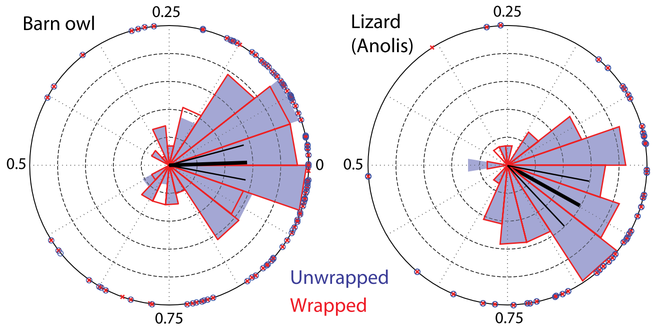

Fig. 3. SFOAE phase accumulation between adjacent SOAE peaks for both owls (left, $L_p = 20$ dB SPL) and lizards (right, $L_p = 30$ dB SPL). Both unwrapped (blue) and wrapped (red) phase conditions are shown. Data are shown both as individual points on the unit circle, as well as (normalized) polar histogram. Also shown is the (mean) resultant vector for the unwrapped condition [thick black radial line (48)], whose length (± angular deviation) was 0.56 ± 0.93 for owl and 0.60 ± 0.89 for lizard. Mean angle (± 95% confidence intervals; thin black radial lines) was 0.005 ± 0.04 cycles for owl and -0.08 ± 0.05 cycles for lizard.

Discussion

We showed here that, despite disparate inner ear morphologies, the ears of barn owls and anoles share key similarities with OAE properties of human ears. Our chief experimental finding is that there is a uniform amount of SFOAE phase accumulation between adjacent SOAE peaks (Fig. 3). We interpret this correlation between spontaneous and evoked emissions, preserved across different vertebrate groups, as indicative of common collective dynamics at work in all ears. We propose that cochlear (i.e., wave-based) model formulations can be generalized to provide a universal thread tying together micro- and macroscopic descriptions. Thereby, these data motivate the need to develop a more comprehensive theoretical foundation to cement our understanding of the salient biomechanics and the collective role hair cells play together.

Recasting Coherent Reflection. Numerous mammalian OAE models have focused around the concept of coherent reflection (CR) (39), describing energy associated with BM traveling waves as scattered across a spatially distributed region about the wave peak, owing to an assumed inherent mechanical roughness. This linear framework has been highly successful and used as both a foundation for a "taxonomy" of OAE generation (15) and as a basis for an SOAE model that likens the mammalian cochlea to a standing wave cavity, roughly analogous to a laser (16). That model predicted a relationship between SOAE spacing and SFOAE phase, which has been verified experimentally (16, 47). Intriguingly, similar predictions are also made by a different class of model, which considers the inner ear as a collection of coupled nonlinear/active oscillators exhibiting nearest-neighbor coupling and ignores BM and stapes reflections (49). The owl and lizard data presented here are consistent with these predictions (Fig. 3), despite morphological differences. For example, although the role of BM traveling waves in the barn owl is presently unknown, such waves are not present in lizards (34, 35). This is not to say that waves are altogether absent in lizard ears: Aside from fast compressional waves that are presumably present in the fluid, other types of waves could arise independent of the BM (13, 50).

Given the uncertain role of traveling waves in nonmammals, do the comparative OAE interrelationships reported here support or refute coherent reflection as a mechanism tied to SOAE generation? To address this question, we argue that coupled nonlinear active oscillator frameworks (11–13) are not fundamentally different from wave-based models (17–19, 51)—the key distinguishing feature is just the assumed form of interelement coupling. That is, wave-based and "local oscillator"-based formulations need not be orthogonal notions. We thereby propose that the basic notion of CR can be cast more universally as one of phase coherence of coupled elements. That is, the crucial notion is that of timing or, for oscillatory conditions, phase (52). The "phase coherence" aspect describes how the individual elements (i.e., active oscillators) do or do not act together in concert (45, 53, 54), whereas the associated biomechanics of how this arises depends upon how the elements are "coupled." Such coupling, hydrodynamically or via passive supporting structures (e.g., tectorial membrane), presumably takes different forms for different morphologies.

Such a hypothesis is broadly consistent with that proposed by Shera (16), who in referring to nonmammalian ears, stated "a slightly irregular array of tuned oscillators, all coupled together … to produce the large mechanical phase shifts concomitant with sharp tuning—may be all that is required for creating global resonances analogous to those evidently responsible for SOAEs in the mammalian ear." More detailed theoretical and computational study is needed to verify this hypothesis (12, 18, 50, 55, 56), develop a rigorous definition of phase coherence (*Supporting Information*), connect such back to cochlear wave-based formulations (e.g., the "scattering integral" of refs. 19, 39, and 45), and clarify the role of irregularity (11, 16, 39, 51). Additionally, further study is required to explain the observation that the mean SFOAE phase accumulation between adjacent SOAE peaks in anoles is slightly less than an integral number of cycles (Fig. 3). We further note that whereas the present focus is the context of OAE generation, the notion of phase coherence of coupled elements is a broader biophysical principle at work in many other contexts, such as stereovillar transduction (57), neural networks (58–60), genetic dynamics (61), and molecular "electronic coherences" thought to be relevant for photosynthetic processes (62).

Entrainment Versus Suppression. A basic unresolved biophysical question is how the underlying oscillators contributing to SOAEs react to an external stimulus. Specifically, are they suppressed (i.e., forced into a quiescent state, such as "amplitude death"; e.g., ref. 63) or entrained (i.e., forced to actively oscillate at the external stimulus frequency; e.g., ref. 5)? The SFOAE measurement "suppression" paradigm (15) provides a basis for distinction. We argue that for Fig. 1*A* (top traces) there was entrainment of some subset of underlying oscillators to the probe (red), which essentially constitute the emission. Such a contribution (or a fraction of such) is subsequently shifted away when a nearby/higher-level suppressor tone was also present (blue). This notion is supported by the observation that the residual depends upon the suppressor: If the frequency is sufficiently far away or the level lower than that of the probe, the residual generally drops toward the noise floor. In fact, the blue traces in Fig. 1*A* suggest complete "suppression" was not achieved. In some rare instances, the SFOAE magnitude was larger than that

of the evoking stimulus, an observation presumably related to facilitation effects (6). Furthermore, SFOAE phase-gradient delays commonly, although not always, showed localized increases about SOAE peaks (e.g., Fig. S6*A*). These are likely telling points, possibly suggesting a strengthened coherence effect from more oscillators (i.e., those on both sides of the SOAE peak) owing to entrainment to the external tone.

Relationship to Neural Responses. A remaining question to address is the nature of how the active oscillators interact with the external tone to produce an SFOAE with a significant delay. That is, what causes the characteristic interference apparent in the top traces of Fig. 1*A* and the phase gradients of Fig. 1*C* (also shown in Fig. 2 *A* and *C*)? Additionally, the mean 0.45-kHz SOAE interpeak spacing for the owl is suggestive of a delay of ∼2.2 ms when viewed in terms of standing wave interference (also note the similarity between N_{SOAE} and N_{SFOAE} in Fig. 2). One plausible explanation is tuning (45, 64). Each underlying oscillator, regardless of whether it is entrained into an SOAE cluster or to an external tone, has both a unique characteristic frequency and selectivity (or filter width, commonly quantified via a *Q*-value). The more sharply tuned a given "filter" is, the slower the corresponding temporal dynamics. Put another way, the delays apparent in the SFOAEs are associated with the build-up time toward steady state of the entrained oscillators behaving in a phase-coherent fashion. Shown in Fig. 2*A* for owls, as previously demonstrated for a variety of mammals (43, 44) and lizards (45), these SFOAE delays correlate well to measures of frequency selectivity at the level of the peripheral ANFs. This similarity suggests that a broader biophysical context where a phase-coherence effect relating tuning of individual elements to that of a collective group is generally insensitive to gross differences in mechanical coupling between hair cells. For the barn owl, the correlation shown in Fig. 2 *A* and *B* supports the notion that tuning can account for most of the delayed nature of SFOAEs. Our data clearly show greater delays for the lowest-level SFOAE measurements. Thus, to optimally compare SFOAE and ANF measures (e.g., Fig. S7) additional study is needed to clarify phase-gradient level dependence across species and the distinction between "isoresponse" and "isolevel" measures (65). Finally, whereas SOAE suppression tuning curves match well to ANF tuning (6, 25), SOAE interpeak spacing does not when compared broadly across species (66), motivating further study.

Methods

Measurements were made in nine owls, whose middle ear was vented (18-gauge needle penetrating through the outer skull into the middle-ear cavity) and six lizards. All animals were lightly anesthetized via injectable agents [owls: ketamine (10 mg/kg) and xylazine (3 mg/kg); lizards: sodium pentobarbital (30 mg/kg)] and body temperatures were stabilized by a heating blanket before recording (39 °C for owls, ∼25 °C for anoles). Animals recovered several hours after the experiment. All work was approved by the authorities of Lower Saxony, Germany (Niedersächsisches Landesamt für Verbraucherschutz und Lebensmittelsicherheit), permit number AZ 33.9-42502-04-13/1182, and by the York University Animal Care Committee (protocol no. 2012-19).

OAE data were collected using identical stimulus paradigms for both species, similar to humans (e.g., Fig. S5 and ref. 47). An Etymotic ER-10C, which contained the two stimulus transducers and measurement microphone, was coupled to the meatus. SFOAEs were evoked by swept tones (41), generally between 1 and 11 kHz, and extracted using a suppression paradigm (15, 40). Probe levels (L_p) varied in different runs from 0 to 50 dB SPL, with a suppressor 15 dB higher in level (L_s) and 40 Hz higher in frequency. Sample rate for all data acquisition was 44.1 kHz. The SOAE spectrum in Fig. 1*A* was obtained by spectrally averaging 60 buffers of 32,768 points each. Spectrograms shown in Fig. 1*B* and Fig. S1*B* were made via short-time Fourier transforms, using a 4,096-point time window with sliding overlap of 97%, and then averaging for the ∼30 sweeps collected during a given SFOAE run. Because SOAE peak frequencies could vary a small amount throughout an experiment [e.g., owing to small temperature fluctuations (25)], we quantified SOAE peak frequencies from the SFOAE sweep waveforms. A 2-dB SNR criterion was used to qualify SOAE peaks, which corresponds visually to the appearance of horizontal bands in Fig. 1*B*. This identification scheme was further validated by examining long time waveforms (120 s) collected before or after the SFOAE run, where more spectral averaging emphasized the rippling/peak structure hinted at in Fig. 1*A*. Additional methodological details are similar to those described previously (15, 22). We define two derived quantities here. First is N_{SFOAE}, which is defined as the product of frequency and the negative of the slope of the (unwrapped) SFOAE phase versus frequency, determined using centered differences (64). Second is N_{SOAE}, which is the geometric mean frequency between two adjacent SOAE peaks divided by their frequency difference (16). Fig. 2 also includes reanalysis of previously published ANF data (29). Data were pooled from 359 units from 13 animals (not the same as those used for the OAE measurements). Neural tuning was quantified as Q_{ERB} from previously measured frequency threshold curves as follows. For each tuning curve, the characteristic frequency (CF) was identified at the minimum decibel SPL for a given tuning curve. The area under the entire tuning curve was then integrated across frequency, after flipping the ordinate, converting to pascals, and squaring, to obtain the equivalent rectangular bandwidth (ERB). The filter quality factor is then $Q_{ERB} = CF/ERB$.

ACKNOWLEDGMENTS. Discussions with A. Salerno, C. Shera, S. Verhulst, and A. Zayed are gratefully acknowledged, as is administrative assistance from M. Caplan and critical input from the reviewers. This work was supported by Deutsche Forschungsgemeinschaft Grant CRC/TRR 31 "Active Hearing" (to C.K.) and Natural Sciences and Engineering Research Council of Canada (C.B.).

1. Freeman DM, Weiss TF (1988) The role of fluid inertia in mechanical stimulation of hair cells. *Hear Res* 35(2-3):201–207.
2. Kozlov AS, Baumgart J, Risler T, Versteegh CP, Hudspeth AJ (2011) Forces between clustered stereocilia minimize friction in the ear on a subnanometre scale. *Nature* 474(7351):376–379.
3. Hudspeth AJ (2008) Making an effort to listen: Mechanical amplification in the ear. *Neuron* 59(4):530–545.
4. Kemp DT (1978) Stimulated acoustic emissions from within the human auditory system. *J Acoust Soc Am* 64(5):1386–1391.
5. Long GR, Tubis A (1988) Investigations into the nature of the association between threshold microstructure and otoacoustic emissions. *Hear Res* 36(2–3):125–138.
6. Manley GA (2001) Evidence for an active process and a cochlear amplifier in nonmammals. *J Neurophysiol* 86(2):541–549.
7. Wit HP (1986) Statistical properties of a strong otoacoustic emission. *Peripheral Auditory Mechanisms*, eds Allen J, et al. (Springer, Berlin), pp 221–228.
8. Crawford AC, Fettiplace R (1985) The mechanical properties of ciliary bundles of turtle cochlear hair cells. *J Physiol* 364:359–379.
9. Talmadge CL, Tubis A, Wit HP, Long GR (1991) Are spontaneous otoacoustic emissions generated by self-sustained cochlear oscillators? *J Acoust Soc Am* 89(5): 2391–2399.
10. Ó Maoiléidigh D, Nicola EM, Hudspeth AJ (2012) The diverse effects of mechanical loading on active hair bundles. *Proc Natl Acad Sci USA* 109(6):1943–1948.
11. Vilfan A, Duke T (2008) Frequency clustering in spontaneous otoacoustic emissions from a lizard's ear. *Biophys J* 95(10):4622–4630.
12. Dierkes K, Lindner B, Jülicher F (2008) Enhancement of sensitivity gain and frequency tuning by coupling of active hair bundles. *Proc Natl Acad Sci USA* 105(48):18669–18674.
13. Gelfand M, Piro O, Magnasco MO, Hudspeth AJ (2010) Interactions between hair cells shape spontaneous otoacoustic emissions in a model of the tokay gecko's cochlea. *PLoS ONE* 5(6):e11116.
14. Kemp DT (1986) Otoacoustic emissions, travelling waves and cochlear mechanisms. *Hear Res* 22:95–104.
15. Shera CA, Guinan JJ, Jr (1999) Evoked otoacoustic emissions arise by two fundamentally different mechanisms: a taxonomy for mammalian OAEs. *J Acoust Soc Am* 105(2 Pt 1):782–798.
16. Shera CA (2003) Mammalian spontaneous otoacoustic emissions are amplitude-stabilized cochlear standing waves. *J Acoust Soc Am* 114(1):244–262.
17. Duke T, Jülicher F (2003) Active traveling wave in the cochlea. *Phys Rev Lett* 90(15):158101.
18. Ku EM, Elliott SJ, Lineton B (2009) Limit cycle oscillations in a nonlinear state space model of the human cochlea. *J Acoust Soc Am* 126(2):739–750.
19. Epp B, Verhey JL, Mauermann M (2010) Modeling cochlear dynamics: Interrelation between cochlea mechanics and psychoacoustics. *J Acoust Soc Am* 128(4):1870–1883.
20. Manley GA (2000) Cochlear mechanisms from a phylogenetic viewpoint. *Proc Natl Acad Sci USA* 97(22):11736–11743.
21. Manley GA, Gallo L (1997) Otoacoustic emissions, hair cells, and myosin motors. *J Acoust Soc Am* 102(2 Pt 1):1049–1055.
22. Bergevin C, Velenovsky DS, Bonine KE (2010) Tectorial membrane morphological variation: Effects upon stimulus frequency otoacoustic emissions. *Biophys J* 99(4): 1064–1072.

23. Bergevin C, Velenovsky DS, Bonine KE (2011) Coupled, active oscillators and lizard otoacoustic emissions. *What Fire is in Mine Ears: Progress in Auditory Biomechanics*, eds Shera CA, Olson ES (AIP Publishing, Melville, NY), pp 453–460.
24. van Dijk P, Manley GA, Gallo L, Pavusa A, Taschenberger G (1996) Statistical properties of spontaneous otoacoustic emissions in one bird and three lizard species. *J Acoust Soc Am* 100:2220–2227.
25. Taschenberger G, Manley GA (1997) Spontaneous otoacoustic emissions in the barn owl. *Hear Res* 110(1-2):61–76.
26. Konishi M (1973) How the owl tracks its prey: Experiments with trained barn owls reveal how their acute sense of hearing enables them to catch prey in the dark. *Am Sci* 61:414–424.
27. Fischer FP, Köppl C, Manley GA (1988) The basilar papilla of the barn owl Tyto alba: A quantitative morphological SEM analysis. *Hear Res* 34(1):87–101.
28. Köppl C, Gleich O, Manley GA (1993) An auditory fovea in the barn owl cochlea. *J Comp Physiol A Neuroethol Sens Neural Behav Physiol* 171:695–704.
29. Köppl C (1997) Frequency tuning and spontaneous activity in the auditory nerve and cochlear nucleus magnocellularis of the barn owl Tyto alba. *J Neurophysiol* 77(1): 364–377.
30. Dyson ML, Klump GM, Gauger B (1998) Absolute hearing thresholds and critical masking ratios in the European barn owl: A comparison with other owls. *J Comp Physiol A Neuroethol Sens Neural Behav Physiol* 182:695–702.
31. Köppl C (1997) Phase locking to high frequencies in the auditory nerve and cochlear nucleus magnocellularis of the barn owl, Tyto alba. *J Neurosci* 17(9):3312–3321.
32. Gummer AW, Smolders JW, Klinke R (1987) Basilar membrane motion in the pigeon measured with the Mössbauer technique. *Hear Res* 29(1):63–92.
33. Miller MR (1981) Scanning electron microscope studies of the auditory papillae of some iguanid lizards. *Am J Anat* 162(1):55–72.
34. Peake WT, Ling A, Jr (1980) Basilar-membrane motion in the alligator lizard: Its relation to tonotopic organization and frequency selectivity. *J Acoust Soc Am* 67(5): 1736–1745.
35. Holton T, Hudspeth AJ (1983) A micromechanical contribution to cochlear tuning and tonotopic organization. *Science* 222(4623):508–510.
36. Bialek W, Wit HP (1984) Quantum limits to oscillator stability: Theory and experiments on acoustic emissions from the human ear. *Phys Lett A* 104:173–178.
37. Long GR, Talmadge CL (1997) Spontaneous otoacoustic emission frequency is modulated by heartbeat. *J Acoust Soc Am* 102(5 Pt 1):2831–2848.
38. Manley GA, Schulze M, Oeckinghaus H (1987) Otoacoustic emissions in a song bird. *Hear Res* 26(3):257–266.
39. Zweig G, Shera CA (1995) The origin of periodicity in the spectrum of evoked otoacoustic emissions. *J Acoust Soc Am* 98(4):2018–2047.
40. Brass D, Kemp DT (1993) Suppression of stimulus frequency otoacoustic emissions. *J Acoust Soc Am* 93(2):920–939.
41. Kalluri R, Shera CA (2013) Measuring stimulus-frequency otoacoustic emissions using swept tones. *J Acoust Soc Am* 134(1):356–368.
42. Dewey JB, Dhar S (2014) Comparing behavioral and otoacoustic emission fine structures. *Proceedings of the 7th Forum Acusticum* (European Acoustics Association, Kraków, Poland).
43. Shera CA, Guinan JJ, Jr, Oxenham AJ (2010) Otoacoustic estimation of cochlear tuning: Validation in the chinchilla. *J Assoc Res Otolaryngol* 11(3):343–365.
44. Joris PX, et al. (2011) Frequency selectivity in Old-World monkeys corroborates sharp cochlear tuning in humans. *Proc Natl Acad Sci USA* 108(42):17516–17520.
45. Bergevin C, Shera CA (2010) Coherent reflection without traveling waves: On the origin of long-latency otoacoustic emissions in lizards. *J Acoust Soc Am* 127(4): 2398–2409.
46. Schairer KS, Ellison JC, Fitzpatrick D, Keefe DH (2006) Use of stimulus-frequency otoacoustic emission latency and level to investigate cochlear mechanics in human ears. *J Acoust Soc Am* 120(2):901–914.
47. Bergevin C, Fulcher A, Richmond S, Velenovsky D, Lee J (2012) Interrelationships between spontaneous and low-level stimulus-frequency otoacoustic emissions in humans. *Hear Res* 285(1-2):20–28.
48. Berens P (2009) CircStat: A MATLAB toolbox for circular statistics. *J Stat Softw* 31:1–21.
49. Wit HP, van Dijk P, Manley GA (2012) A model for the relation between stimulus frequency and spontaneous otoacoustic emissions in lizard papillae. *J Acoust Soc Am* 132(5):3273–3279.
50. Epp B, Wit H, van Dijk P (2015) Clustering of cochlear oscillations in frequency plateaus as a tool to investigate SOAE generation. *Mechanics of Hearing*, eds Karavitaki KD, Corey DP (AIP Publishing, Melville, NY), in press.
51. Fruth F, Jülicher F, Lindner B (2014) An active oscillator model describes the statistics of spontaneous otoacoustic emissions. *Biophys J* 107(4):815–824.
52. Rosenblum MG, Pikovsky AS, Kurths J (1996) Phase synchronization of chaotic oscillators. *Phys Rev Lett* 76(11):1804–1807.
53. Müller-Wehlau M, Mauermann M, Dau T, Kollmeier B (2005) The effects of neural synchronization and peripheral compression on the acoustic-reflex threshold. *J Acoust Soc Am* 117(5):3016–3027.
54. Keefe DH (2012) Moments of click-evoked otoacoustic emissions in human ears: Group delay and spread, instantaneous frequency and bandwidth. *J Acoust Soc Am* 132(5):3319–3350.
55. Pikovsky A, Rosenblum M, Kurths J (2000) Phase synchronization in regular and chaotic systems. *Int J Bifurcat Chaos* 10:2291–2305.
56. Roongthumskul Y, Shlomovitz R, Bruinsma R, Bozovic D (2013) Phase slips in oscillatory hair bundles. *Phys Rev Lett* 110(14):148103.
57. Nam JH, Fettiplace R (2008) Theoretical conditions for high-frequency hair bundle oscillations in auditory hair cells. *Biophys J* 95(10):4948–4962.
58. Eckhorn R, et al. (1988) Coherent oscillations: A mechanism of feature linking in the visual cortex? Multiple electrode and correlation analyses in the cat. *Biol Cybern* 60(2):121–130.
59. Mormann F, Lehnertz K, David P, Elger CE (2000) Mean phase coherence as a measure for phase synchronization and its application to the EEG of epilepsy patients. *Physica D* 144:358–369.
60. Lakatos P, Karmos G, Mehta AD, Ulbert I, Schroeder CE (2008) Entrainment of neuronal oscillations as a mechanism of attentional selection. *Science* 320(5872):110–113.
61. Uriu K, Morelli LG (2014) Collective cell movement promotes synchronization of coupled genetic oscillators. *Biophys J* 107(2):514–526.
62. Hayes D, Griffin GB, Engel GS (2013) Engineering coherence among excited states in synthetic heterodimer systems. *Science* 340(6139):1431–1434.
63. Ahn KH (2013) Enhanced signal-to-noise ratios in frog hearing can be achieved through amplitude death. *J R Soc Interface* 10(87):20130525.
64. Shera CA, Guinan JJ, Jr, Oxenham AJ (2002) Revised estimates of human cochlear tuning from otoacoustic and behavioral measurements. *Proc Natl Acad Sci USA* 99(5): 3318–3323.
65. Eustaquio-Martín A, Lopez-Poveda EA (2011) Isoresponse versus isoinput estimates of cochlear filter tuning. *J Assoc Res Otolaryngol* 12(3):281–299.
66. Manley GA, Köppl C, Bergevin C (2014) Common substructure in otoacoustic emission spectra of land vertebrates. *Mechanics of Hearing*, eds Karavitaki D, Corey DP (AIP Publishing, Melville, NY), in press.